Electronic Supplementary Material (ESI) for Lab on a Chip.

Generation of stable orthogonal gradients of chemical concentration and substrate stiffness in a microfluidic device

S. García, R. Sunyer, A. Olivares, J. Noailly, J. Atencia and X. Trepat

Supplementary Movie

Supplementary movie 1: Full view of the buried channel during the scattering assay. At *t*=0h, HGF begins to flow in the main channel and the gradient starts its formation.

Supplementary Figures

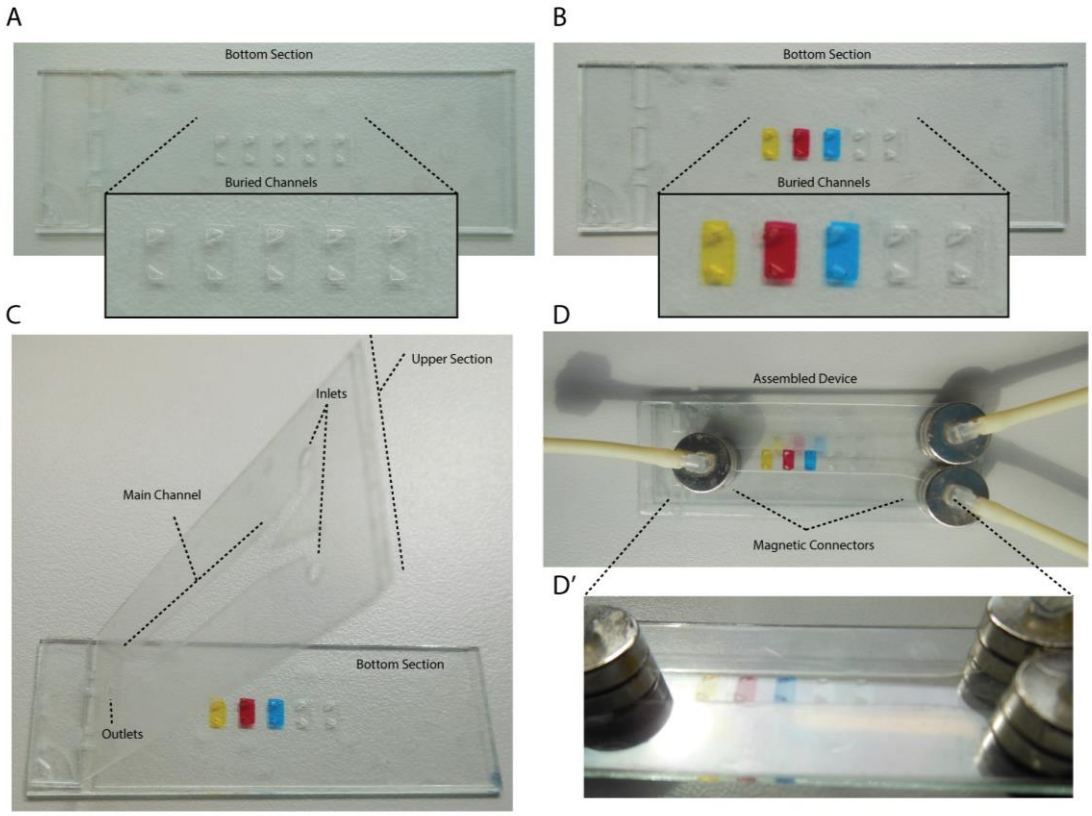

Supplementary Fig. S1. Device Assembly. A) The bottom section is composed of buried channels (bearing PAA gels) and triangular shaped vias. B) Vias allow loading cell suspension, here represented by dye solution in the first three buried channels. C) Upper section, formed by the main channel and inlet/outlet ports, is adhered to the bottom section. D) and D') Different views of the fully assembled device including magnetic connectors.

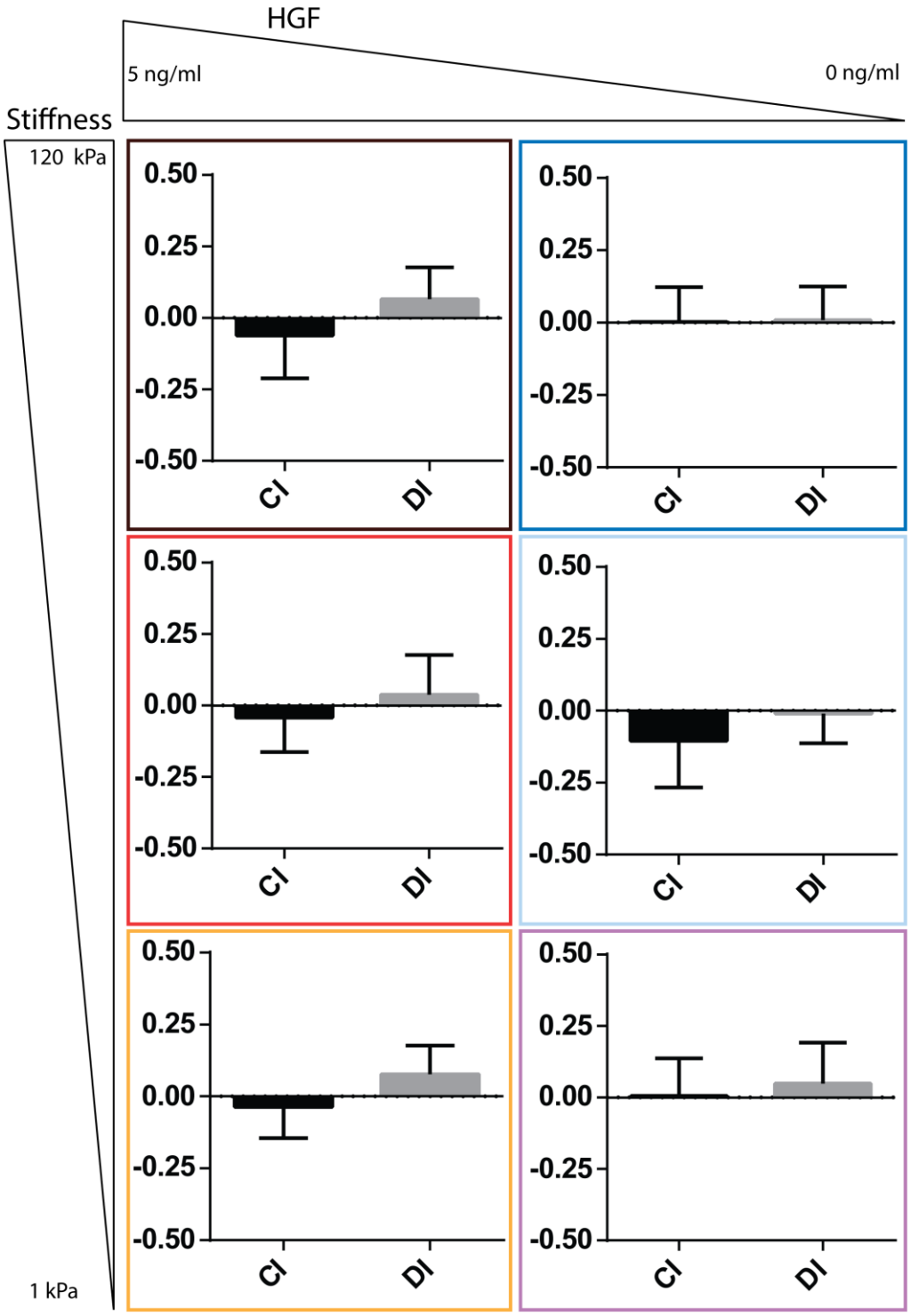

Supplementary Fig. S2. Absence of directional motion in the scattering assay. The composite graph shows the chemotactic index (CI, along HGF gradient) and the durotactic index (DI, along the stiffness gradient) for scattering cells in the six conditions described in the main text (color coded as Fig. 3A and 3B). In all cases cells show directional indices close to zero. Data are represented as Mean ± SD.

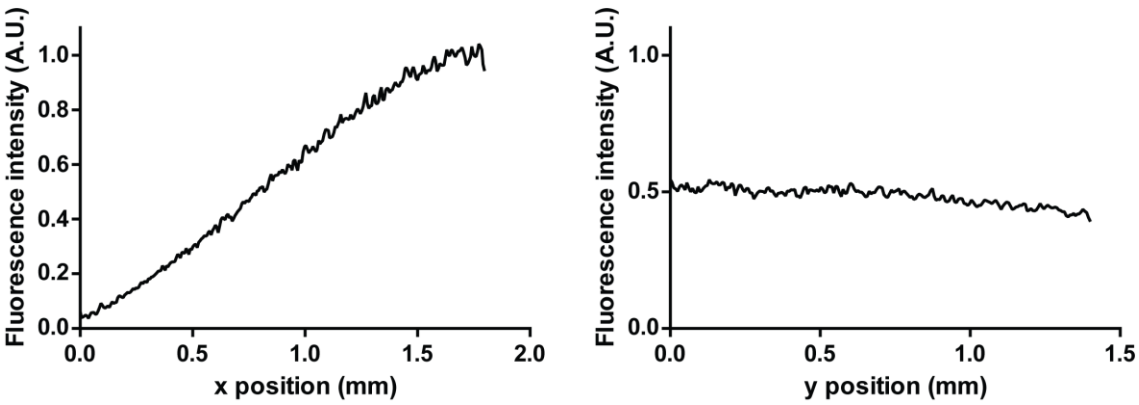

Supplementary Fig. S3. Robustness and stability of a gradient with FITC-dx 70 kDa after 22h. A) Relative fluorescence intensity along the longitudinal axis of the buried channel. B) Relative fluorescence intensity along the transverse axis of the buried channel.

Supplementary Note 1: Hydrodynamic modelling of the microfluidic system

Objectives and Methods

We developed a 3D hydrodynamic model to ensure that 1) the chemical gradient created in our device was predominantly diffusive rather than convective, and 2) whether the gradient is robust against imperfections in the fabrication of the device, especially with regard to the symmetry of the triangular vias.

The 3D model incorporates the part of the main channel connected to the buried channel. Both channels are mutually orthogonal and connected to each other through triangular openings (vias) located at each end of the buried channel (Supplementary Fig. S4). The fluid phase is represented with a viscosity of 0.001 Pa·s and a density of 1000 kg/m^3. The simulated inflow fluid velocity is 40 μm/s, corresponding to the inlet flows of 7 μL/min imposed experimentally, and the outflow pressure is nil. The analysis is performed under steady state flow conditions using Fluent 12.1 (ANSYS). Both the inflow and outflow conditions are applied at the level of the main channel. Zero fluid velocity (no slip condition) is assumed at the walls of the channels and the vias.

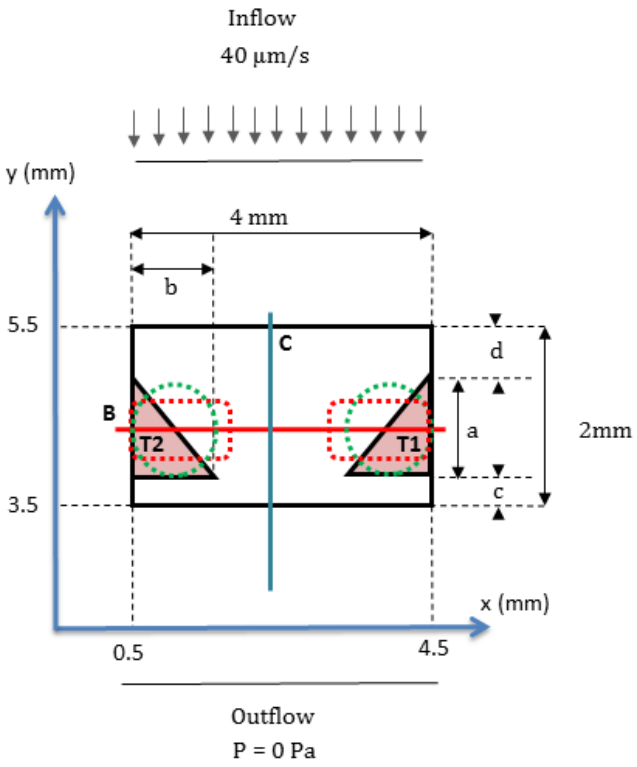

Supplementary Fig. S4. Schematic upper view of the modelled portion of the microfluidic chamber: C lies within the mid-longitudinal plane of the main channel (or within the mid-transversal plane of the buried channel), B runs along the buried channel, and T1 and T2 are the two triangular vias. In some simulations, the triangular vias were replaced by circular or rectangular ones with same cross-sectional area (dashed green and red lines respectively).

Modelled walls are rigid and impermeable. Fluid velocity, fluid pressure, fluid shear stress (FSS), and Reynolds (Re) and Peclet (Pe) numbers are computed. For the Pe calculations, we consider a diffusivity of 1.10^{-10} m^2/s, in order to represent the diffusion of molecules of about 10 kDa. Wall shear stress predictions are also possible, leading to an estimation of the fluid-induced stimulation that the cells attached to the chamber material may feel.

We run computational fluid dynamic (CFD) simulations in four different scenarios: one ideally symmetric chamber model (Original), and three asymmetric chamber models (Asy1-3) obtained through changes of the dimensions of one triangular opening, i.e. T2, while the opposite opening keeps its original dimensions (Supplementary Fig. S4 and Table S1). Dimensional variations introduced to generate the Asy models are estimated based on empirical knowledge about the outcome of the chamber manufacture. All models are meshed with the same kind and similar amount of elements, i.e. about 160 000 tetrahedral elements (Table S1). To study the dependence of the device's hydrodynamics on the shape of the vias we simulate flow patterns with circular or rectangular vias rather than triangular ones. To do so, the values of the cross-sectional area and the distance d, as defined for the perfectly symmetric models with the triangular vias (Supplementary Fig. S4), are kept constant.

Models	a (mm)	b (mm)	c (mm)	d (mm)	# Tetrahedral element
Original	1.4	1	0.2	0.4	162 730
Asy1	1.26	0.9	0.2	0.54	161 975
Asy2	1.4	1	0.34	0.26	166 586
Asy3	1.26	0.9	0.34	0.4	162 924

Table S1: Specific characteristics of the four microfluidic chamber models: dimensions of T2 (Supplementary Fig. S4), as defined in the original and in the three asymmetric models, and number of elements used to mesh each model.

Results and discussion

As shown in Supplementary Fig. S5, the flow simulated through the main channel invades the triangular vias down to the extremities of the buried channel, being able to feed these extremities with the solutes injected in the main channel. Moreover, Supplementary Fig. S6A reveals that the fluid velocities in most of the buried channel are one order of magnitude lower than at the extremities, independently on the type of asymmetry simulated. As for the detail of the fluid velocity magnitudes along C (Supplementary Fig. S6B), the full symmetry (Original) always yields the lowest fluid velocity values. Shifting T2 with respect to T1 (Asy2) in the direction of the fluid in the main channel leads to higher fluid velocity values than when T2 is distorted. The fluid velocity predictions in the buried channel result in maximum wall shear stress values that do not overcome 0.16 mPa nearby the openings, and decrease below 0.02 mPa in the central part of the channel. These values are far below the values of the order of 1-10 Pa usually felt by vascular endothelial cells[1].

The calculated Reynolds number does not overcome Re = 0.004, either in the main or in the buried channels, confirming that the model assumptions lead to the laminar regime (Re < 1) expected in the microfluidic device. Supplementary Fig. S7 shows the distribution of the Peclet number calculated across the buried channel. Pe is always >1 at the level of T1 and T2 (Supplementary Fig. S7A). In contrast, Pe was < 1 in most of the buried channel's length, independently on the simulated asymmetry. Thus transport within the buried channel is largely diffusive, even when T2 is shifted with respect to T1 (Asy2) (Fig. S7A,B).

[1] Fisher, a B., Chien, S., Barakat, a I., & Nerem, R. M. (2001). Endothelial cellular response to altered shear stress. American *Journal of Physiology. Lung Cellular and Molecular Physiology*, 281, L529–L533.

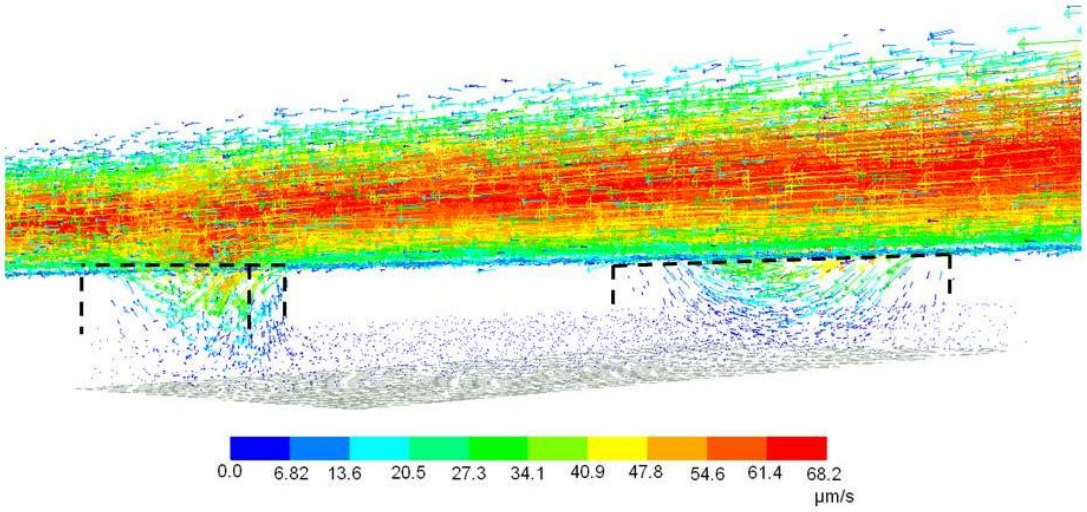

Supplementary Fig. S5. 3D representation of the fluid velocities calculated within the fully symmetric microfluidic chamber (Original model). Vias are marked with dashed lines. The main and buried channels appear in the upper and lower parts of the figure, respectively.

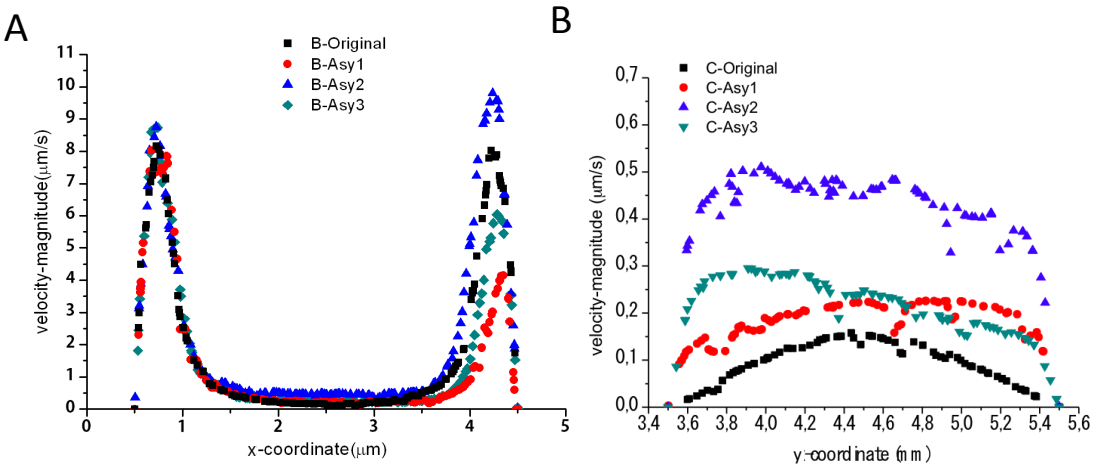

Supplementary Fig. S6. Distributions of total fluid velocity calculated within the buried channel for the symmetric and the three different asymmetric models (Table S1), along B (A), and along C (B) – Axes B and C are represented in Supplementary Fig. S4.

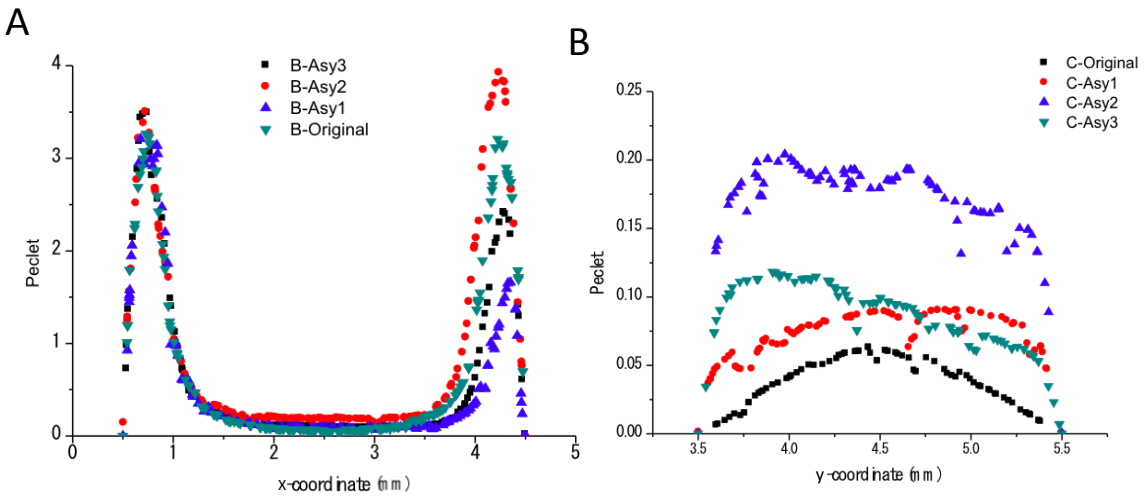

Supplementary Fig. S7. Pe values calculated throughout the buried chamber for the symmetric and the three different asymmetric models (Table S1), along B (A), and along C (B) – Axes B and C are represented in Supplementary Fig. S4.

As for the influence of the vias geometry, all shapes (triangular, circular and rectangular, see Fig. S4) led to relatively low fluid velocities and most of the fluid within the buried channel was characterized by Pe numbers lower than 1. In all cases, the Pe dropped quickly below 0.30 in the immediate vicinity of the vias. In contrast to vias that are symmetric with respect to the mid-longitudinal axis of the buried channel, triangular vias accommodate the loss of pressure of the fluid trapped along the y-axis by progressively recruiting larger volumes of fluid from the main channel. This effect improved the symmetry of the fluid velocity distributions through the width of the buried channel (Supplementary Fig. S8), but was not translated into a diffusive zone larger than those achieved with the other vias. Many more geometrical variations could have been simulated for the vias. However results strongly suggest that the concept of the buried channel, perpendicular and laterally connected to the main channel is per-se efficient enough to generate a pure diffusive zone under the fluid simulated conditions.

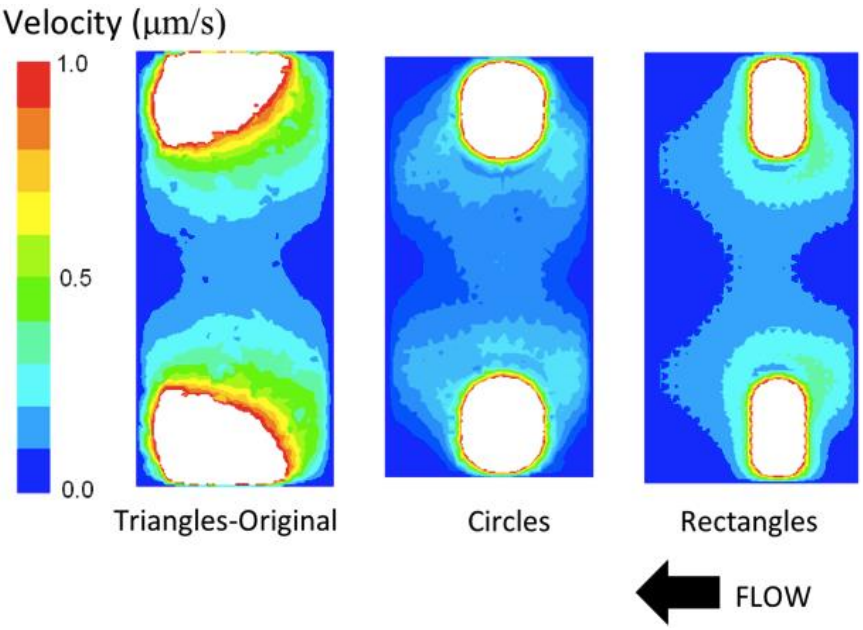

Supplementary Fig. S8. Colour map of fluid velocity distributions in the mean plane of the buried channel for triangular, circular, and rectangular vias.